Proceedings of the ASME-JSME-KSME 2019 Joint Fluids Engineering Conference
AJKFLUIDS2019
July 28-August 1, 2019, San Francisco, CA, USA

AJKFLUIDS2019-5223

BUBBLE MEASUREMENT VIA HOUGH TRANSFORM IN HIGHLY OVERLAPPING CONDITIONS

Thomas Shepard[1]
University of St. Thomas
Saint Paul, MN

Thomas Höft
University of St. Thomas
Saint Paul, MN

ABSTRACT

Accurate measurement of bubble size in digital images can prove challenging in conditions that involve significant overlapping of bubbles and/or images with a combination of in and out of focus bubbles. The method employed in the current study uses the circular Hough transform to identify circular features in the image. This method can handle mildly non-circular (i.e. non-spherical) bubbles as well as non-trivial overlapping. Several image pre-processing steps are employed to improve the method's accuracy in detecting in-focus bubbles along with their radii, reduce both spurious detection of out-of-focus bubbles and non-bubble features, and reduce non-detection of in-focus bubbles. Pre-processing steps include histogram equalization and illumination variation reduction via filtering. In this paper, results from the algorithm are compared against a manual detection of bubbles in digital images under conditions of varying bubble diameter and bubble number density.

Keywords: bubble diameter, Hough transform, digital image

INTRODUCTION

Bubbles serve an important role in a large variety of applications such as waste water treatment, heat transfer enhancement, chemical reactors, effervescent atomization, drag reduction and aeration of water bodies and during the brewing process, just to name a few. For most applications, the size of the bubbles and/or size distribution can affect performance. Thus, researchers in the bubbly two-phase arena frequently require a means of measuring the size of bubbles.

Previous researchers have demonstrated a variety of techniques for measuring bubble size. Some of these methods require the use of intrusive probes that physically can interact with bubbles such as capillary suction [1-2], optical fiber [3-4] and resistance probes [5-6]. Phase Doppler anemometry systems are capable of measuring bubbles [1] though require the bubbles to be spherical and of sufficiently small number density.

One method that avoids some of these pitfalls is capturing digital images of the bubbles and then using an image processing algorithm to extract relevant bubble measurements from the image. The advancement of digital camera capabilities and computational speeds of computers makes this technique increasingly attractive. Though it is noted that digital image processing techniques present challenges that can be difficult to overcome in a robust manner without requiring significant user input. Common challenges can include images that have both focused and unfocused bubbles, bubbles that overlap and variable background brightness which could also affect contrast. As most clear spheres suspended in a clear medium and backlit will provide very similar looking digital images, relevant literature need not be restricted to bubbles. Algorithms that have been developed for liquid sprays in particular can be informative for algorithms intended for bubbles, and vice versa.

There are many methods available for determination of whether an object is in-focus or not in a digital image. Some of the more commonly used methods involve the calculation of local pixel intensity gradients in an image [7-9] or the pixel contrast in relation to the image background [10-11]. These techniques are commonly built into image processing software and can require user input to specify a threshold or sensitivity. For example, MATLAB has seven built in edge detection methods that operate using various intensity gradient criteria for recognizing an in-focus edge. Bubble size and size distribution in combination with the depth of field of the imaging optics are also relevant to focus. For a shallow depth of field, a large bubble is more likely to have part of its volume in-focus than a smaller bubble. This makes it possible for measurements made via image processing to bias towards larger objects [12].

[1] Contact author: Thomas.shepard@stthomas.edu

The recognition of edges, or areas of an image that are in-focus, is commonly an early step in a multi-step algorithm for identifying and measuring bubbles. Dealing with overlapping objects is another common step and many methods have been reported. For images with low number density of spherical bubbles one technique involves the removal of non-circular objects using a shape factor criteria [8, 11, 13]. For more heavily overlapping images, the identification of arcs on object perimeters and their assignment to individual bubbles allows for missing sections of the object to be filled in algorithmically [14]. This method has also been employed with elliptical bubbles [15-16]. The use of template matching has also been demonstrated where a template image, or images can be marched through an image while looking for regions of strong correlation [17]. Cruvinel et al. [18] have employed a similar technique after applying a Fourier transform and then examining correlations in the frequency domain. It is noted that as algorithm sophistication increases, and particularly for marching methods, the computational requirements can become significant. Further, as bubble density increases in an image, algorithms developed for images with less overlapping and cleaner backgrounds can become unreliable [19].

In this paper, a method for automatically identifying and measuring bubbles based on the circular Hough transform [20] is presented. The circular Hough transform has been successfully used for locating and measuring droplets, particles, and micro-scale assembly components [21-25]. Several image processing steps prior to the Hough transform are employed that improve the quality and robustness of bubble detection and measurement. The number of user-selected parameters is small, and we provide values for the imaging conditions described herein. A comparison is made between the results of the algorithm and results from manual measurement. Finally, the strengths and limitations of our method are discussed.

EXPERIMENTAL PROCEDURE

The bubble images used in the current study were taken of bubbles flowing through a 10 mm x 10 mm cross section channel. Air was injected through porous plates into a cross flow of 3% saltwater solution. To change the average bubble diameter and number density of bubbles within an image, the liquid flow rate, air flow rate and/or porous media grade could all be varied. A NikonD-7000 camera was used in conjunction with a Navitar 12X zoom lens to capture images of 4928 x 3264 pixel resolution. The zoom level was such that 607 pixels was equal to 1 mm. Shadowgraphy images were taken by backlighting the bubbles and using an IET Labs 1546 Strobotac with a 2 μs flash that was diffused via tracing paper. More details about the experimental set-up can be found in [26].

In total, eight different bubble conditions were examined as shown in Fig. 1. These represented four nominally different bubble sizes that existed at a higher and lower number density within an image. For this paper we designate the four bubble sizes using the terms: Large (Fig. 1A-B), Medium-Large (Fig. 1C-D), Medium-Small (Fig. 1D-F) and Small (Fig. 1 G-H). The density difference is also shown in Fig. 1 with the left hand column showing the Higher Density (HD) condition and the right hand column showing the Lower Density (LD) condition.

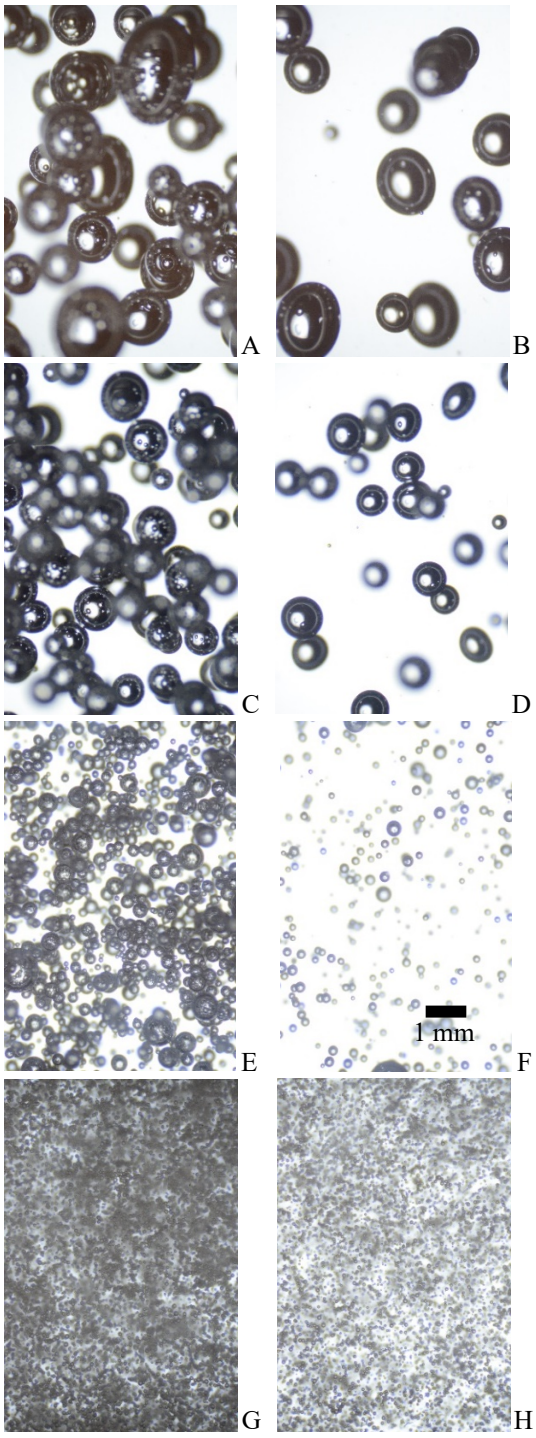

FIGURE 1: Range of conditions studied showing variety in bubble diameter and number densities. The scale in F applies to all images.

In order to provide a comparison for the algorithm employed in this study, bubbles were also measured using a manual line drawing method. Black lines were drawn on the bubbles that were considered in-focus and a MATLAB code then measured these lines. This technique involves judgment on the part of the user and it is noted that different users could disagree as to what would constitute in-focus. This personal judgment results in uncertainty in the bubble measurement using the line drawing technique that has previously been documented as ±8% for average bubble diameter and ±5% for bubble diameter standard deviation [27]. For the different bubble conditions shown in Fig. 1, multiple images were processed using both the manual line method and the circular Hough transform algorithm for comparison.

IMAGE PROCESSING ALGORITHM

The goal in this work is to develop a mostly automatic image processing algorithm in Matlab to identify bubble locations and diameters using relatively few user-selected parameters and which could easily be run on a large batch of images. The image processing algorithm presented here is composed of three major steps. The first step is a pre-processing step, the second determines which portions of the image are in focus, and the third uses the circular Hough transform to identify circular features in the image. Below each of these steps is described in detail and their function is illustrated. For a logic tree summarizing the algorithm, see Fig. 2.

The pre-processing step removes small amounts of noise, and in the case of high number density, emphasizes the boundaries of bubbles where there are regions with significant overlapping of bubbles. This latter case employs flat field correction, histogram equalization, and Gaussian smoothing while the former employs only Gaussian smoothing. The Gaussian smoothing step serves to reduce random fluctuations in the image pixel values arising from noise in the camera circuitry. Since the later steps of the algorithm use large changes in image pixel value to identify the edges of bubbles, noise in the image will be incorrectly identified as bubble edge, and negatively impact bubble detection. Gaussian smoothing is computed by low-pass filtering the image with a 2-D Gaussian function of user-determined standard deviation σ_G [20], resulting in a smoothed image I_σ. We use Matlab's built-in *imgaussfilt* function with σ_G depending on the bubble conditions. For small bubbles we use σ_G =2 pixels and for the remaining cases we use σ_G =10 pixels. Fig. 3B illustrates the effect of smoothing; notice that the bubble edges have become less sharp, as one would expect with a low-pass filter. While blurring the sharp edges seems counterproductive to identifying these features, in practice the degree of blur is outweighed by the reduction in noise.

Flat field correction reduces variation in illumination across an image by estimating the illumination and removing it via simple division. The illumination estimation is simply a Gaussian-smoothed version of the image. For small bubbles we use standard deviation σ_F =100 pixels and for the remaining cases we use standard deviation σ_F =200 pixels. That is, the

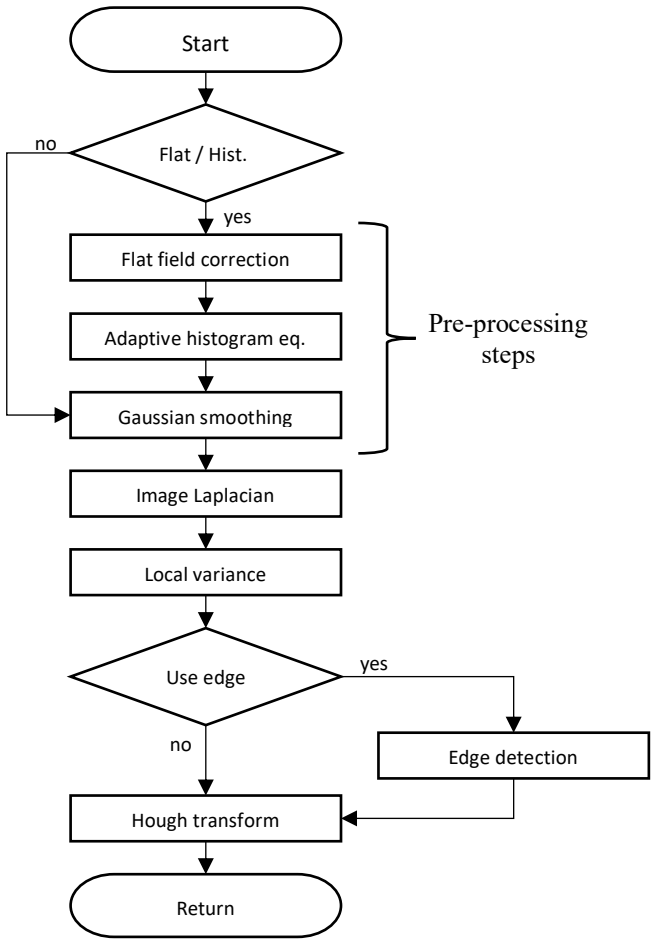

FIGURE 2: Logic tree summarizing the algorithm.

smoothing is performed of a much larger region of the image than the noise removal above. The noise removal is meant to reduce local fluctuations in pixel value while the flat field correction is meant to reduce larger scale fluctuations in the image arising from a reduction in light transmission through regions with high density of bubbles. Notice that in Figs. 1E and 1G some portions of the image are darker than others. We denote the image as I and the Gaussian-smoothed image as I_G. The flat field corrected image is then I / I_G where the division is done pixel-by-pixel. Matlab's built-in function *imflatfield* was used for this step.

Histogram equalization increases contrast in an image by transforming the histogram of image pixel values so that the histogram becomes approximately flat. We apply an adaptive equalization which, in contrast to traditional global equalization, equalizes the histogram on sub-portions of the image [28], using Matlab's built-in function *adapthisteq*. Figure 3C shows the combined effect of flat field correction, adaptive histogram equalization and Gaussian smoothing. We denote the pre-processed image, whether using all three steps or only smoothing, by I_{pre}.

Following these preprocessing steps, the algorithm identifies which portions of the image are in focus. The goal is

to only detect and measure circles in the image corresponding to in-focus bubbles and ignore circles from out-of-focus bubbles. A simple way to estimate whether a pixel in an image is in focus is via the local variance of the image Laplacian [29]. To compute the image Laplacian, a discrete second derivative, we convolve, or filter, the pre-processed image I_{pre} with the 3x3 matrix

$$L = \begin{bmatrix} 0 & -1 & 0 \\ -1 & 4 & -1 \\ 0 & -1 & 0 \end{bmatrix},$$

resulting in the image I_L. The image Laplacian varies more in regions where the image consists of rapid changes in pixel value, as at the edge of an in-focus bubbles, and varies less in regions of less change, as at the edge of an out-of-focus bubble. At each pixel of I_L the variance of the pixel values of I_L is computed in a small window about that pixel. The size of the window varies with the size of the bubbles, from $w_L = 11$ pixels for the smallest, $w_L = 21$ pixels for medium sizes, and $w_L = 31$ pixels for the largest. The image formed by these local variances of the Laplacian is denoted I_{var}. Examples of I_L and I_{var} are shown in Figs. 3D-E.

In some cases, the image I_{var} is used as the input to the circular Hough transform; in other cases, an edge detection step is first performed, and the result is used as the input to the Hough transform. For the edge detection the Canny detector in Matlab with two thresholds [20] was used. The upper threshold selects strong edges, and the lower threshold discards weak edges. We uniformly use 0.25 for the upper and 0.02 for the lower threshold. We denote the resulting image I_{edge}. See Fig. 3F for an example of I_{edge}.

The above image processing steps serve to prepare the original image for analysis by the circular Hough transform[2] [20]. The Hough transform is a voting-based method for locating and measuring circular features in an image. We use a Matlab implementation via the built-in function *imfindcircles*. Within the *imfindcircles* function, the input image is first converted to a binary image by thresholding the image gradient. This simple edge detection process assigns pixels near large image intensity changes and likely to be part of objects of interest the value 1, leaving uninteresting pixels with value zero. The Hough transform then loops through circles of all possible centers and diameters and queries each pixel of value 1 to determine if it is part of each of those circles. If yes, this is a vote that a pixel at location (i, j) is part of a putative circle at center c_k with diameter d_l. Circles with total vote accumulation above a user-determined threshold are considered present in the image; the Matlab function returns a list of centers and radii, which are converted to diameter. We refer to the binary threshold as τ_B and the voting, or sensitivity, threshold as τ_S. In the Matlab function *imfindcircles*, a larger value for τ_S corresponds to a more sensitive detection, which is equivalent to a *lower* value of the voting threshold.

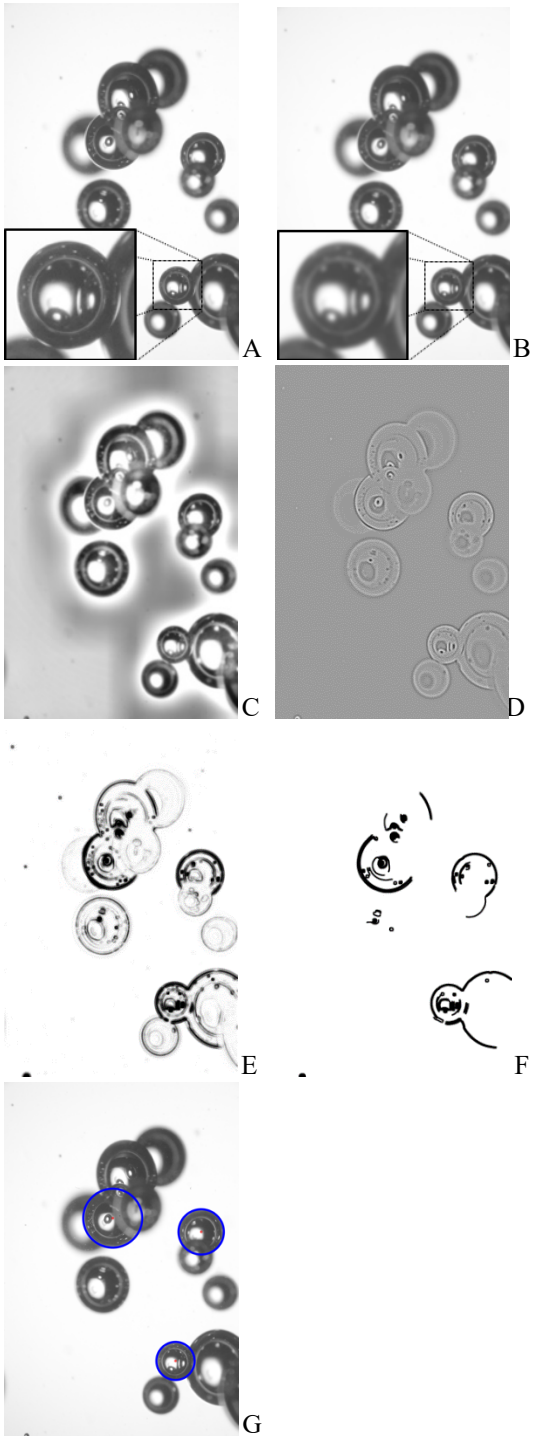

FIGURE 3: Steps in the image processing algorithm. A: original image I. B: Gaussian-smoothed I_σ. C: I_{pre} after all three pre-processing steps. D: Image Laplacian I_L. E: Local variance of the image Laplacian I_{var} (contrast enhanced). F: Edge-detection image I_{edge}. G: Original image with detected circles overlaid.

[2] The "circular Hough transform" is related to the "Hough transform," with the latter detecting straight lines and the former detecting circles. For brevity, since we do not use the (linear) Hough transform in this work, in this paper we refer to the circular Hough transform as simply the Hough transform.

Values for all image processing parameters are provided in Table 1 where the first column represents the bubble condition as shown in Fig. 1 (LHD = large, higher density; MSHD = medium-small, lower density, etc.).

	σ_G	σ_F	w_L	τ_S	τ_B	flat/hist	I_{var}/ I_{edge}
LHD	10		31	0.98	0.20	no	edge
LLD	10		31	0.90	0.15	no	var
MLHD	10	100	41	0.97	0.10	yes	edge
MLLD	10		21	0.90	0.10	no	var
MSHD	10	200	21	0.90	0.10	yes	edge
MSLD	10		21	0.65	0.15	no	var
SHD	2	100	11	0.90	0.10	yes	var
SLD	2		11	0.90	0.10	no	var

TABLE 1: Parameter values used for different bubble conditions. The column "flat/hist" indicates with "yes" that all three pre-processing steps are used; "no" indicates that only Gaussian smoothing is used in which case σ_F is not used. The column "I_{var} / I_{edge}" indicates which image is used as input to the Hough transform

As illustrated in Fig. 3G, visual inspection indicates that our algorithm generally performs reasonably well. We discuss here some qualitative strengths and weaknesses of the algorithm. See the Results section below for quantitative comparison with manually obtained measurements.

The algorithm successfully identifies in-focus bubbles and provides an accurate measurement of bubble diameter. It is able to handle several challenging scenarios that are difficult even for manual measurement. For example, in Fig. 3G a large in-focus bubble is partially occluded by another bubble, has a bubble behind it, and only a partial arc of the circle is visible, but the method is able to accurately identify and measure this bubble. The algorithm is also able to measure some bubbles which are partially or mostly out of the image frame, as shown on the right edge of Fig. 4A; a manual diameter measuring method might not be able to measure such a bubble.

Choice of the Hough transform thresholds is a trade-off between detecting as many in-focus bubbles as possible and rejecting non-bubble features in the image. In Fig. 4B one can see both non-detected bubbles and detection and measurement of features which clearly do not correspond to in-focus bubbles (e.g. blue circle filled with only white background). In particular, when a gap between bubbles is approximately or partially circular, this gap may be incorrectly identified as an in-focus bubble. Both non-detection and spurious detection can be thought of as noise on the histogram of bubble sizes. In all conditions, there are more small non-bubble circular features than large ones. Both gaps between bubbles, bubbles lensed through in-focus bubbles, and the inner boundary of the bubble are smaller than the bubbles themselves (Fig. 4D). Thus, spurious detection is biased towards smaller bubbles, and we expect that measure bubble size distributions may skew towards smaller sizes than manual measurement.

While our algorithm is able to handle somewhat distorted (non-spherical) bubbles as shown in the center and inset of Fig. 4C, we observe two issues. First, detection of non-circular features requires a higher sensitivity (larger τ_S) which can result in more detection of spurious features. Second, even with lower sensitivity, a bubble which has been flattened but still has circular/spherical ends may be detected as two separate smaller bubbles. This is shown in Fig. 4C where a circular bubble is detected at the bottom edge of a larger elliptical bubble.

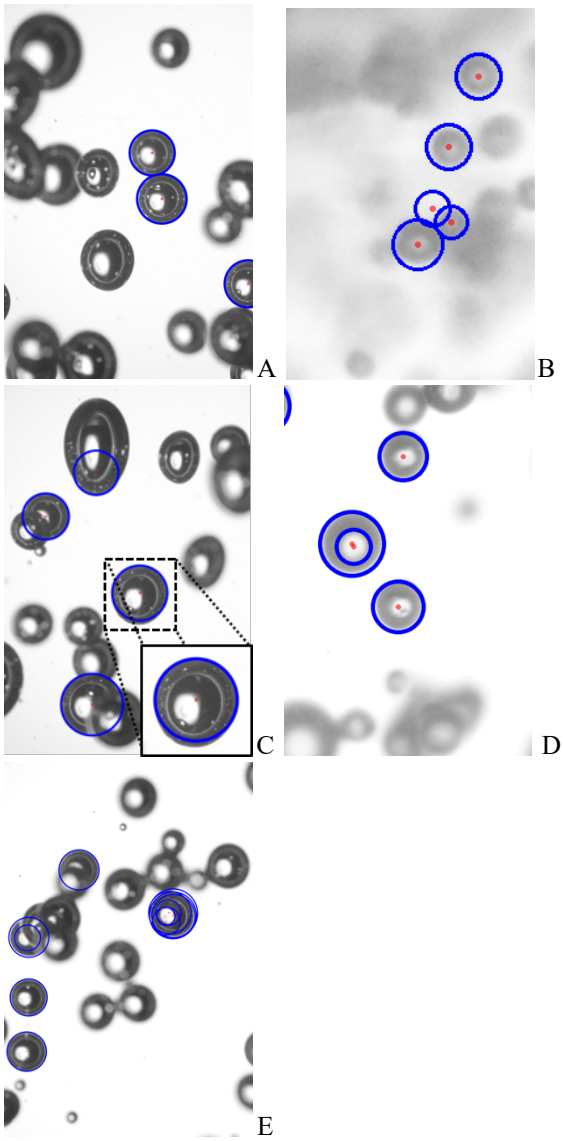

FIGURE 4: A: Detection of a partially out-of-frame bubble. B: Non-detection of bubbles and spurious detection of a gap between bubbles (zoom). C: Detection of non-spherical bubbles, both spurious (upper) and genuine (center & inset). D: Spurious detection of multiple bubbles with similar centers but different diameters (zoom). E: Spurious detection of multiple bubbles with similar centers and similar diameters.

Finally, the Hough transform is fundamentally sensitive to noise. Small changes in the pixels considered by the voting accumulation can have a large impact on the set of detected circles. Our algorithm attempts to minimize this effect by incorporating a robust set of pre-processing steps from denoising

to in-focus determination. One effect of setting τ_S too large (very sensitive detection of circles) is over-detection of circular features. In Fig. 4E, one bubble is detected multiple times because several circles were plausible given the edge-detected pixels and voting threshold. Reducing τ_S can alleviate this issue but may result in failing to detect the other bubbles in the image.

Table 1 presents the parameter values used for all processing steps for each of the operating conditions. The same parameter values are used for all bubble sizes within a given image and image set; a future improvement would be to tailor the parameters to bubble size not just across conditions but within each image. One strength of the method is the small number of parameters (five or six, depending on the pre-processing method, plus choice of edge or variance as input to the Hough transform). A drawback of the method is that the results are somewhat sensitive to choice of parameter value. In particular a small change in the Hough transform thresholds can lead to failure to detect in-focus bubbles, or spurious detection of non-bubbles. Fortunately, the remaining parameter values are quite robust.

RESULTS

The algorithm parameters listed in Table1 were selected by starting with a value to achieve a desired effect and then refining the value through trial-and-error coupled with visual inspection of the results on a subset of bubble images for each condition. For example, σ_G was initially selected to be on the order of the number of pixels in the transition from white background to dark in-focus foreground for a bubble; this value was larger for larger bubbles than for smaller bubbles, but caused too much blurring in large bubbles, so the value was reduced until it had the desired effect of reducing noise but not introducing extraneous blur. Similarly, w_L, the window over which the variance of the image Laplacian is computed, was selected to be large enough to encompass a bubble edge and the region around it but not so large as to include neighboring bubbles or bubbles lensed through the interior. The Hough transform parameters τ_S and τ_B were also determined via trial-and-error process, using the Matlab default values as a starting point: τ_S = 0.85, τ_B automatically selected using Otsu's method [20].

A few trends can been seen in the finalized algorithm parameters as shown in Table 1. Generally, pre-processing with both flat-field correction and histogram equalization was used in higher-density images to enhance contrast between in-focus bubbles and the background of out-of-focus images but omitted in lower-density images since it was unnecessary. Edge-detection as input to the Hough transform was more useful in higher density conditions. Three parameters were clearly dependent on bubble size: σ_G, σ_F, and w_L. The exception is the medium-large higher density case, which had a high degree of lensing and bubble overlap obscuring in-focus bubbles, making this a very challenging case. The parameter values chosen here, while being more the result of trial and error than selection from principles in order to achieve an effect, can provide useful guidance for others implementing algorithms for a similar range of bubble image conditions.

A comparison of the average bubble diameter (D_{b_avg}) found using the line drawing technique and Hough transform algorithm is shown in Fig. 5. These data represent the average diameter measured for an image set at the various bubble conditions shown in Fig. 1. Examination of the data shows reasonable agreement between the algorithm and manual measurement technique. The average deviation between the techniques is 13% (averaged over all cases presented), which is larger than the uncertainty in the manual measurement. However, depending on the application this level of uncertainty may be deemed acceptable given the time savings involved with use of the algorithm in processing a large batch of images in comparison to the manual method. Figure 5 also demonstrates an interesting phenomenon in that the algorithm tends to underestimate the average population diameter for higher number density images and overestimate the diameter for lower number densities.

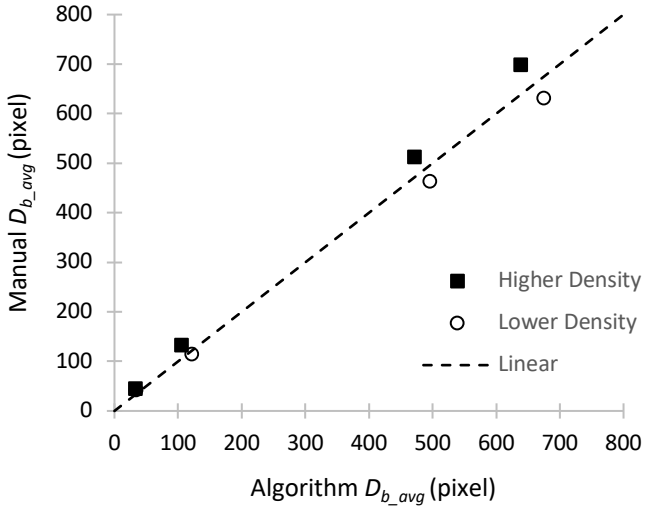

FIGURE 5: Comparison of manual and algorithm determined average bubble diameter.

In order to better understand how the Hough transform algorithm measurements compare against the manual method, size distributions are shown in Figs. 6-9. In these images, the black lines correspond to the higher number density condition while the gray lines are for the lower number density. In addition, the solid lines correspond to the manual measurement method while dashed lines represent data from the code incorporating the Hough transform algorithm. The y-axis of these plots, frequency, represents the decimal equivalent of the % of the population that has a given bubble diameter.

An examination of these images reveals that for each bubble condition the manual measurement method captures a broader distribution of bubble sizes than the Hough transform algorithm. The exact reasons for this have not been distilled yet and are likely caused by a number of factors including the detection of false bubbles and the measureable diameter restrictions that are inherent to the algorithm. In essence, the user directs the Hough transform to look for bubbles in a certain diameter range. If that

range is extended too low, for a given condition, the number of spurious bubbles detected increases. This effect is seen in Figs. 6-9 whereby the bubbles sizes detected by the code do not show a gradual tailing off at lower diameters.

One implication for this disagreement is for higher order population statistics such as the Sauter mean diameter. For seven of the eight conditions examined the manual diameter measurement resulted in a larger Sauter mean diameter with an average deviation of 26% as compared to the Hough transform algorithm.

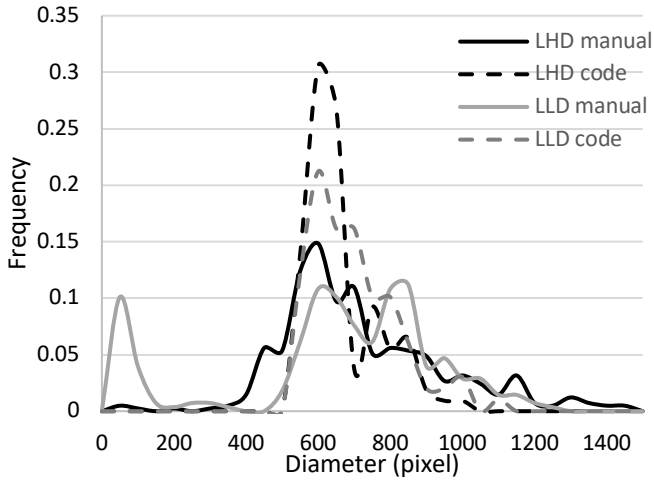

FIGURE 6: Bubble size distributions for Large bubbles as measured via manual line method and image processing code for higher and lower number density conditions.

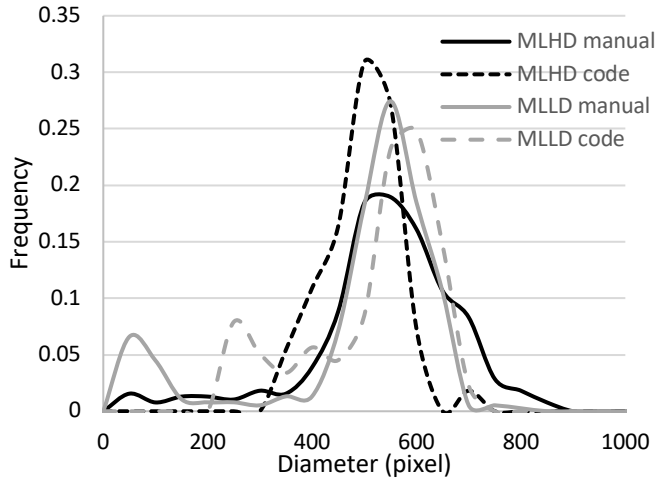

FIGURE 7: Bubble size distributions for Medium-Large bubbles as measured via manual line method and image processing code for higher and lower number density conditions.

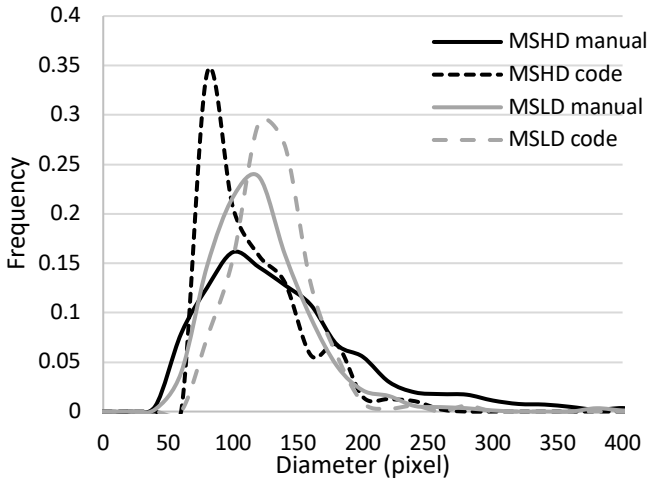

FIGURE 8: Bubble size distributions for Medium-Small bubbles as measured via manual line method and image processing code for higher and lower number density conditions.

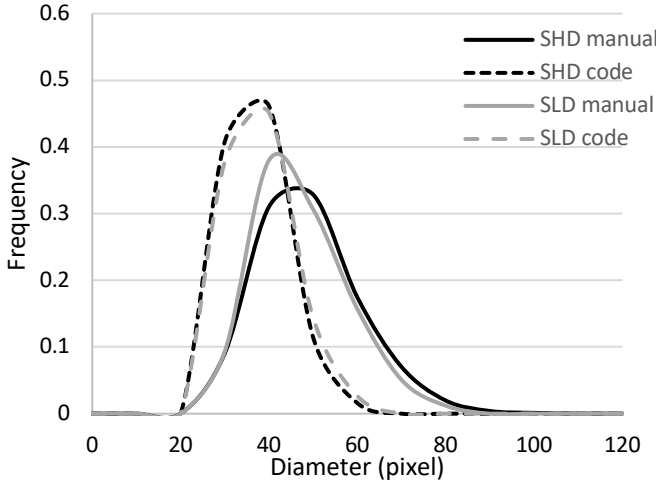

FIGURE 9: Bubble size distributions for Small bubbles as measured via manual line method and image processing code for higher and lower number density conditions.

CONCLUSION

The ability to accurately and automatically determine bubble diameters from images can be a difficult objective except under limited conditions. For bubble images which present a range of bubble sizes, significant overlapping, variable background intensity and a vast range of bubble focus (in-focus vs. out-of-focus) it can be straightforward for the human eye to spot what is measureable but much more difficult to create an algorithm to do so. In this study an algorithm for measurement of bubble diameters in digital images has been detailed including the steps for preprocessing and the relevant user-defined parameters. This algorithm was then compared against a manual measurement technique for eight bubble conditions that are particularly challenging.

The algorithm shows promise and demonstrated an ability to detect which bubbles were in focus and determine their diameter even when much of the bubble was obscured by other bubbles or cropped by the edge of the image. While the algorithm compared reasonably well with the manual measurement in terms of average bubble diameter it showed limitations in capturing the population distribution. The detailed description of the algorithm and provided parameters provide a useful starting point for enhancements in the functionality and accuracy of the algorithm. The current work is distinguished from much of the relevant literature in two ways. First, the basic algorithm was applied to an incredibly wide range of bubble conditions that varied in size, eccentricity, amount of overlapping and number density. Second, this work details how algorithm inputs are dependent on this range of bubble conditions.

Future efforts for improving the algorithm are focused on two main avenues. The first is the detection of a greater number of bubbles in an image as there were some images where it was unclear why some seemingly in-focus bubbles were left undetected. As greater detection will also result in an increase in spurious detections, the second avenue for improvement will focus on rejection of spurious bubbles. In particular, an average bubble intensity threshold may be utilized to discard bubbles detected in the background of the image due to the curvature of nearby bubbles (see Fig. 4B). Further, a comparison of bubble centroid position and diameter can be implemented to address the issue of multiple bubbles incorrectly being detected in a given region (see Fig. 4D-E).

ACKNOWLEDGEMENTS

The authors wish to acknowledge the efforts of Eric Ruud, Henry Kinane and Jeremiah Bonde in taking the images used for this work and manually measuring the bubbles.

NOMENCLATURE

σ_G	Pre-processing Gaussian filter standard deviation
σ_F	Pre-processing adaptive histogram Gaussian filter standard deviation
w_L	Window size for local variance of image Laplacian
τ_S	Sensitivity parameter for Hough transform
τ_B	Threshold for edge detector in Hough transform
D_{b_avg}	Average bubble diameter
I	Original image
I_σ	Gaussian-smoothed image
I_{pre}	Image following (one or three) pre-processing steps
I_L	Result of applying image Laplacian to I_{pre}
I_{var}	Result of computing local variance on I_L
I_{edge}	Edge image of I_{var}
LHD	Large bubble, higher density condition
LLD	Large bubble, lower density condition
MLHD	Medium-large bubble, higher density condition
MLLD	Medium-large bubble, lower density condition
MSHD	Medium-small bubble, higher density condition
MSLD	Medium-small bubble, lower density condition
SHD	Small bubble, higher density condition
SLD	Small bubble, lower density condition

REFERENCES

[1] Laakkonen, M., Moilanen, P., Miettinen, T., Saari, K., Honkanen, M., Saarenrine, P., Aittamaa, J., 2005, "Local bubble size distributions in agitated vessel: comparison of three experimental techniques," Chemical Engineering Research and Design, 83(1), pp.50-58.

[2] Hernandez-Aguilar, J.R., Coleman, R.G., Gomez, C.O., Finch, J.A., 2004, "A comparison between capillary and imaging techniques for sizing bubbles in flotation systems," Minerals Engineering, 17, pp. 53-61.

[3] Saberi, S., Shakourzadeh, K., Bastoul, D., Militzer, L., 1995, "Bubble size and velocity measurement in gas-liquid systems: Application of fiber optic technique to pilot plant scale," The Canadian Journal of Chemical Engineering, 73(2), pp. 253-257.

[4] Besagni, G., Brazzale, P., Fiocca, A., Inzoli, F., 2016, "Estimation of bubble size distributions and shapes in two-phase bubble column using image analysis and optical probes," Flow Measurement and Instrumentation, 52, pp. 190-207.

[5] Roesler, T.C., 1988, "An experimental study of aerated-liquid atomization," Ph.D. Thesis, Purdue University, West Lafayette, IN.

[6] Liu, T.J., Bankoff, S.G., 1993, "Structure of air-water bubbly flow in a vertical pipe – II. Void fraction, bubble velocity and bubble size distribution," International Journal of Heat and Mass Transfer, 36(4), pp. 1061-1072.

[7] Fantini, E., Tognotti, L., Tonazzini, A., 1990, "Drop size distribution in spray by image processing," Computers & Chemical Engineering, 14(11), pp. 1201-1211.

[8] Lecuona, A., Sosa, P.A., Rodriguez, P.A., Zequeira, R.I., 2000, "Volumetric characterization of dispersed two-phase flows by digital image analysis," Measurement Science and Technology, 11, pp. 152-1161.

[9] Xu, C., Shepard, T.G., 2014, "Digital Image Processing Algorithm for Determination and Measurement of In-Focus Spherical Bubbles," Proceedings of ASME Fluids Engineering Division Summer Meeting 2014, FEDSM2014-21187.

[10] Kim, K.S., Kim, S.S, 1994, "Drop sizing and depth-of-field correction in TV imaging," Atomization and Sprays, 4, pp. 65-78.

[11] Malot, H., Blaisot, J.B., 2000, "Droplet size distribution and sphericity measurements of low-density sprays through image analysis," Particle & Particle Systems Characterization, **17**(4), pp. 146-158.

[12] Koh, K.U., Kim, J.Y., Lee, S.Y., 2001, "Determination of in-focus criteria and depth of field in image processing of spray particles," Atomization and Sprays, 11(4), pp. 317-333.

[13] Kim, G., Lee, S.Y., 1990, "A Simple Technique for Sizing and Counting of Spray Drops Using Digital Image Processing," Experimental. Thermal and Fluid Science, 3(2), pp. 214-221.

[14] Kim, Y.D., Lee, S.Y., Chu, J.H., 2001, "Separation of Overlapped Particles Using Boundary Curvature Information," Proceedings of the 6th Annual Conference on Liquid Atomization and Spray Systems, pp. 259-264.

[15] Honkanen, M., Saarenrinne, P., Stoor, T., Niinimake, J., 2005, "Recognition of highly overlapping ellipse-like bubble images," Measurement Science and Technology, 16, pp. 1760-1770.

[16] Zhang, W.H., Jiang, X., Liu, Y.M., 2012, "A method for recognizing overlapping elliptical bubbles in bubble image," Pattern Recognition Letter, 33, pp. 1543-1548.

[17] Zabulis, X., Papara, M., Chatziargyriou, A., Karapantsios, T.D., 2007, "Detection of densely dispersed spherical bubbles in digital images based on a template matching technique Application to wet foams," Colloids and Surfaces A: Physiochem. Eng. Aspects, 309, pp. 96-106.

[18] Cruvinel, P.E., Vieira, S.R., Crestana, S., Minatel, E.R., Mucheroni, M.L., Neto, A.T., 1999, "Image Processing in Automated Measurements of Raindrop Size and Distribution," Computers and Electronics in Agriculture, 23, pp. 205-217.

[19] Zhong, S., Zou, X., Zhang, Z, Tian, H., 2016, "A flexible image analysis method for measuring bubble parameters," Chemical Engineering Science, 141, pp. 143-153.

[20] Gonzalez, R., Woods, R., 2008, "Digital Image Processing," 2nd ed., Prentice Hall.

[21] Peng, T., Gupta, S., Balijepalli, A., LeBrun, T., 2006, "Algorithms for on-line monitoring of components in an optical tweezers-based assembly cell," Proceedings of ASME IDETC/CIE, Paper No. DETC2006-99546.

[22] Khalil, A., Puel, F., Chevalier, Y., Galvan, J.-M., Rivoire, A., Klein, J.-P., 2010, "Study of droplet size distribution during an emulsification process using *in situ* video probe coupled with automatic image analysis," Chemical Engineering Journal, 165, pp. 946-958.

[23] Lee , S. Y., Kim, Y. D., 2004, "Sizing of spray particles using image processing technique," KSME International Journal, 18(6), pp. 879-894.

[24] Kruis, F.E., Denderen, J.V., Burrman, H., Scarlett, B., 1994, "Characterization of agglomerated and aggregated aerosol particles using image analysis," Particle & Particle Systems Characterization, 11(6), pp. 426-435.

[25] Kim, H., Lee, S.Y., 2002, "Application of Hough transform to image processing of heavily overlapped particles with spherical shapes," Atomization and Sprays, 12(4), pp. 451-461.

[26] Shepard, T., Ruud, E., Kinane, H., Law, D., Ordahl, K., 2018, "Bubble Formation From Porous Plates in Liquid Cross-Flow," Proceedings of ASME FEDSM 2018, Paper No. FEDSM2018-83221.

[27] Shepard, T.G., 2011, "Bubble size effect on effervescent atomization," Ph.D. thesis, University of Minnesota, Minneapolis, MN.

[28] Zuiderveld, K. 1994, "Contrast Limited Adaptive Histograph Equalization" in *Graphic Gems IV*, Heckbert, P., ed., Academic Press, pp. 474–485.

[29] Pertuz, S., Puig, D., Garcia, M., 2013, "Analysis of focus measure operators for shape-from-focus," Pattern Recognition, 46(5), pp. 1415-1432.